3190–3203 *Nucleic Acids Research, 2016, Vol. 44, No. 7* *Published online 28 January 2016*
doi: 10.1093/nar/gkw034

Rad61/Wpl1 (Wapl), a cohesin regulator, controls chromosome compaction during meiosis

Kiran Challa[1], Min-Su Lee[2], Miki Shinohara[1], Keun P. Kim[2] and Akira Shinohara[1,*]

[1]Institute for Protein Research, Graduate School of Science, Osaka University, 3-2 Yamadaoka, Suita, Osaka 565-0871, Japan and [2]Department of Life Sciences, Chung-Ang University, Seoul 156-756, Korea

Received June 19, 2015; Revised January 5, 2016; Accepted January 12, 2016

ABSTRACT

Meiosis-specific cohesin, required for the linking of the sister chromatids, plays a critical role in various chromosomal events during meiotic prophase I, such as chromosome morphogenesis and dynamics, as well as recombination. Rad61/Wpl1 (Wapl in other organisms) negatively regulates cohesin functions. In this study, we show that meiotic chromosome axes are shortened in the budding yeast *rad61/wpl1* mutant, suggesting that Rad61/Wpl1 negatively regulates chromosome axis compaction. Rad61/Wpl1 is required for efficient resolution of telomere clustering during meiosis I, indicating a positive effect of Rad61/Wpl1 on the cohesin function required for telomere dynamics. Additionally, we demonstrate distinct activities of Rad61/Wpl1 during the meiotic recombination, including its effects on the efficient processing of intermediates. Thus, Rad61/Wpl1 both positively and negatively regulates various cohesin-mediated chromosomal processes during meiosis.

INTRODUCTION

During DNA replication, sister chromatids are tightly connected with each other through the activity of a protein complex named cohesin (1,2). Sister chromatid cohesion (SCC) plays a critical role not only in chromosome segregation but also in the repair of double-strand breaks (DSBs) during vegetative growth (1). The cohesin complex of budding yeast, *Saccharomyces cerevisiae*, is composed of two structural maintenance of chromosome (SMC) ATPases, Smc1 and Smc3 (1,2). The Smc1–Smc3 dimer associates with a kleisin subunit, Scc1/Mcd1 (Rad21 in other eukaryotes), forming a ring. Scc1 interacts with Scc3/Irr1 (SA1/2), a non-SMC subunit. It is commonly accepted that the cohesin complex ring structure embraces two sister chromatids (3), although another model, which does not involve topological trapping of DNA by cohesin ring, was proposed (4). Cohesin provides the physical connection between two sister chromatids, which creates tension at the kinetochores and counteracts the pulling force generated by the microtubules (1). At the onset of anaphase, cohesion is dissolved through the Scc1 subunit cleavage by a cysteine–protease called separase, which enables the release of the entrapped chromatids (5). The separase activation is tightly controlled during the cell cycle by securin, a separase inhibitor and the degradation of securin is regulated through ubiquitination by the anaphase-promoting complex/cyclosome (APC/C) (6).

Loading of the cohesin complex predominantly occurs in G1 phase and it is promoted by the Scc2–Scc4 cohesin loader. During S-phase, the complex is converted into an active cohesion form, possibly as a consequence of the DNA replication fork progression. The cohesin complex activity is positively modulated by Eco1/Ctf7 acetyltransferase-mediated acetylation of the Smc3 subunit (7,8). Eco1 binds to the DNA replication apparatus and promotes S-phase-specific acetylation of Smc3. Additionally, the cohesin function is negatively regulated by two proteins, Pds5 and Rad61/Wpl1 (Wapl in other organisms) (9–11). Eco1-dependent Smc3 acetylation counteracts the negative activity of Rad61/Wpl1 on cohesin chromosome binding. Excluding Rad61/Wpl1, all other cohesin complex subunits are essential for cell viability.

In meiotic cells, SCC along the chromosome arms plays an essential role for the faithful segregation of homologous chromosomes during meiosis I, while SCC in the centromere-proximal regions ensures the correct segregation of sister chromatids during meiosis II (1,12). Chromosome arm cohesion and physical connection between homologous chromosomes, which is cytologically visualized as a chiasma, provide a structural basis for generation of the tension between homologous chromosome axes containing a pair of the replicated sister chromatids. At the onset of anaphase I, the destruction of this arm cohesion promotes the separation of homologous chromosomes to the opposite poles. On the other hand, the cohesin complex at kinetochores is protected by the Shugoshin/MEI-S322 (Sgo1) protein and PP2A phosphatase, which in turn provides physical linkage between sister chromatids in meiosis II (13).

*To whom correspondence should be addressed. Tel: +81 6 6879 8624; Fax: +81 6 6879 8626; Email: ashino@protein.osaka-u.ac.jp

Contrary to the mitotic cohesin complex, the meiotic form of this complex contains a unique subunit (14). In all eukaryotes that have the ability to carry out meiosis, Scc1/Mcd1/Rad21 is replaced with a different member of kleisin family, Rec8 (15). In the budding yeast, Rec8 is meiosis-specific, while other organisms contain different compositions of cohesin components specialized for meiosis (14). Mammals additionally have a second meiosis-specific kleisin Rad21L (16,17).

In addition to the role in cohesion in anaphases I and II, the cohesin complex has other roles, unique to the meiotic prophase I. This complex is a fundamental component of the chromosome axes in meiosis (15) and it is involved in diverse biochemical reactions. The cohesin complex promotes the formation of a meiosis-specific tripartite chromosome structure called the synaptonemal complex (SC) through shaping of the axis structure, axial/lateral elements, with multiple chromatin loops emanating from the axes (15). In the SCs, two parallel axial/lateral elements are connected through the transverse filaments (18) and the two homologous chromosomes are tightly synapsed. Additionally, during meiotic recombination, Rec8, and consequently the cohesin complex, regulates the DSB formation as well as the maintenance of homolog bias (15,19–20).

Although the role of the Rec8 protein in different meiotic processes is well defined (15,19–20), the roles of other cohesin complex components in meiotic prophase I are largely unknown. In this study, we characterize the role of Rad61/Wpl1 during meiosis. Rad61/Wpl1 plays a role in various processes such as SC formation, telomere dynamics and meiotic recombination. Most importantly, in the absence of Rad61/Wpl1, meiotic chromosomes show hypercompaction compared with the wild-type chromosomes, indicating a role of Rad61/Wpl1 in limiting chromosome axis compaction. These data suggest that Rad61//Wpl1 is not only a negative regulator of the cohesin function but also plays a positive role in meiotic chromosome metabolism.

MATERIALS AND METHODS

Strains and strain construction

All strains described here are derivatives of SK1 diploid strains, NKY1551 (*MATα/MAT***a**, *ho::LYS2/″*, *lys2/″*, ura3/″, *leu2::hisG/″*, *his4X-LEU2-URA3/his4B-LEU2, arg4-nsp/arg4-bgl*) and MSY831/832 (*MATα/MAT***a**, *ho::LYS2/″, lys2/″, ura3/″, leu2::hisG/″, trp1::hisG/″*). Parental strain used for the two-dimensional (2D) analyses is KKY276 (19). Strain genotypes are given in Supplementary Table S1. Rap1-GFP and Mps3-GFP have been described previously (21,22). Both of the Green Fluorescent Protein (GFP) fusion proteins are biologically functional, and spore viability of the tagged strains is normal (21,22). *CEN5-GFP* (*CEN5* with TetO array with TetR-GFP) and *CEN4-GFP/TEL4-GFP* were provided by Drs Kim Nasmyth (23) and Doug Koshland (24), respectively. *The rad61:KanMX6* strain was constructed using polymerase chain reaction (PCR)-based tagging methodology (25).

Antisera and antibodies

For immunostaining of proteins involved in the recombination, rabbit anti-Dmc1 and guinea pig anti-Rad51 were used as described previously (26). Anti-Zip1, anti-Red1 and anti-Rec8 antisera for cytology and western blotting have been described previously (27,28). Secondary antibodies conjugated with Alexa488 and Alexa594 dyes (Molecular Probes, Life Technologies, UK) were used for the detection of the primary antibodies.

Cytology

Immunostaining of chromosome spreads was performed as described previously (26,29). Stained samples were observed using an epi-fluorescence microscope (BX51; Olympus, Japan) with a 100× objective (NA1.3). Images were captured by CCD camera (CoolSNAP; Roper, USA), and afterward processed using IP lab and/or iVision (Sillicon, USA), and Photoshop (Adobe, USA) software tools. For statistical analysis of Rad51/Dmc1 quantity, we employed the Mann–Whitney U-test, a non-parametric method, given that the distribution of the results of our experiments did not follow normal distribution.

High-resolution images of the Rap1-GFP and Mps3-GFP localization were obtained by a computer-assisted fluorescence microscope system (DeltaVision, Applied Precision, USA) with an oil immersion objective lens (100×, NA = 1.35). Image deconvolution was carried out using an image workstation (SoftWorks; Applied Precision, USA).

Cohesion and pairing assays

Following fluorescence microscope imaging, the number of chromosomal locus-marked GFP foci in a single cell was counted manually. For the observations of chromosome segregation in meiosis I, cells with two DAPI bodies were selected and the number of GFP foci in each DAPI body was counted.

Pairing of chromosomes was analyzed in the whole yeast cells with two homologous LacI-GFP spots at *CEN5* locus as described previously (24).

Compaction assay

For distance measurements on probed SCs at 0, 4 and 5 h, chromosome spreads were prepared as described above and stained with both anti-Rec8 and anti-GFP antibodies. The distance between two GFP foci on chromosome IV was measured by Velocity™ program (Applied Precision, USA) or IPLab (Sillicon, USA).

Chromatin immunoprecipitation (ChIP)

Chromatin immunoprecipitation (ChIP) was carried out as previously described (30). Briefly, cells were fixed with 2% formaldehyde. Cell lysates were prepared as described (31). Magnetic beads coated with anti-Rec8 antibodies were incubated with the lysates. After an overnight incubation, the beads were recovered and washed extensively. Total DNA was extracted using phenol/chloroform mixture and further purified with ethanol precipitation. Of the purified DNA,

1/10th was used for real-time PCR reactions (BioRad iCycler) with SYBR Green dye (Molecular Probes, Life Technologies, UK). Five sets of paired primers were used in these experiments. Primers for the *CEN* and *CAR* loci are described in Supplemental Table S2.

Fluorescence intensity measurement

Mean fluorescence of the whole nucleus was quantified with Image J. Quantification was performed using unprocessed raw images and identical exposure time setting in DeltaVision system (Applied Precision, USA). The area of a nuclear spread was defined as an oval, and the mean fluorescence intensity was measured within this area.

Fluorescence intensity line profiles were calculated using maximum intensity projections from unprocessed raw images acquired using DeltaVision with the SoftWoRx Line profile tool. Reference lines were drawn so that they intersected with single chromosomes, and intensity per pixel was quantified.

Chromatin fractionation

Chromatin fractionation was performed as described previously (32). The cells were digested with Zymolyase 100T and the spheroplasts were pelleted. The pellets were resuspended in five volumes of hypotonic buffer (HB; 100 mM MES-NaOH, pH 6.4, 1 mM ethylenediaminetetraacetic acid (EDTA), 0.5 mM $MgCl_2$) supplemented with a protease inhibitor cocktail (Sigma, USA). After 5 min, 120 μl of whole cell extract (WCE) were layered onto 120 μl of 20% (W/V) sucrose in HB and centrifuged for 10 min at 16 000 *g*. The supernatants were saved and the pellets were resuspended in 120 μl EBX buffer (50 mM HEPES-NaOH, pH 7.4, 100 mM KCl, 1 mM EDTA, 2.5 mM $MgCl_2$, 0.05% Triton X100) and centrifuged for 10 min at 16 000 *g*. The pellets were again collected and resuspended in EBX buffer with 5 units/ml DNase I and 1 mM $MgCl_2$ for 5 min. The supernatants were saved for further analysis.

Yeast culture

Yeast cell culture and time-course analyses of the events during meiosis and the cell cycle progression were performed as described previously (33,34).

Physical analysis of meiotic recombination

Genomic DNA preparation and physical analysis of recombination were performed as described previously (19,35–36). For 2D gel electrophoresis, genomic DNA was digested with 80 units of XhoI enzyme, and loaded onto 0.4% SeaKem Gold agarose gel in Tris-Borate-EDTA (TBE) buffer, at ∼1 V/cm for 21 h. Gels were stained with 0.5 μg/ml ethidium bromide (EtBr) for 30 min, and afterward the lanes containing DNA of interest were cut out to prepare gel slices. Following this, SeaKem LE agarose (0.8%) with 0.5 μg/ml EtBr was added to the 2D gel tray. The second gel electrophoresis was carried out at ∼6 V/cm, for 6 h at 4°C. Southern blot analysis was performed using ^{32}P-dCTP–labeled radioactive nucleotides, prepared with the Random Primer labeling kit (Agilent Technologies, USA). DNA hybridization signals were quantified using a Bio-Rad Phosphorimager and Quantify One software (Bio-Rad, USA). Detection of DSBs in the *rad50S* background was performed as described previously (19).

RESULTS

Rad61/Wpl1 is necessary for meiosis

Cohesin function is regulated by a non-essential subunit Rad61/Wpl1 (Wapl in other organisms) (9,37). Rad61/Wpl1 is known to negatively regulate SCC by destabilization of the function of cohesin (9–11), but its meiotic functions have not been studied. In order to elucidate the roles of Rad61/Wpl1 in meiosis, a deletion mutant of the *RAD61/WPL1* gene in the SK1 background was constructed. The *rad61/wpl1* mutant cells showed spore viability of 83.8%, which was significantly reduced compared with 98.3% viability in wild-type cells (Figure 1A; chi-square; $P = 7.8 \times 10^{-13}$). Progression of meiosis I was detected by counting the DNA bodies in the cells stained with DAPI. The *rad61/wpl1* mutant displayed a 1.5 h delay in the time to meiosis I relative to the wild-type cells (Figure 1B), suggesting a possible role of Rad61/Wpl1 in meiotic prophase I. Western blotting analyses of the expression of various meiotic marker proteins showed that the *rad61/wpl1* cells demonstrate a delay in Zip1 and Rec8 disappearance in addition to a delay in cleavage of Rec8 in comparison with wild-type cells (Figure 1C). This suggests a delayed exit from prophase I.

In order to determine whether Rad61/Wpl1 is involved in SCC during meiotic prophase I, yeast cells heterozygous for Cen5-GFP were analyzed for proficient SCC (23). While SCC normally produces a single Cen5-GFP focus per nucleus, defective SCC generates two foci (Figure 1D). To eliminate the effect of meiosis I (MI), we introduced an *ndt80* mutation, which induces pachytene arrest (38). In these strains, the resolution of two GFP foci results from sister chromatid separation and not MI chromosome segregation. At 4 h, among the wild-type cells (*ndt80* mutant), ∼90% of cells had a single Cen5-GFP focus indicating proficient SCC at Cen5, whereas 9.2% of cells showed two Cen5-GFP foci (Figure 1E). In the *rad61/wpl1* mutant cells, 72.3% of cells had a single Cen5-GFP focus with an increase in the number of cells with two Cen5-GFP foci to 27.7% (chi-square; $P = 3.1 \times 10^{-10}$), indicating a partial defect in SCC in *rad61/wpl1* cells arrested a the mid-pachytene stage.

Using the same Cen5-GFP construct, we analyzed the frequency of the pairing of the chromosomal loci in cells homozygous for Cen5-GFP in the *ndt80* background (Figure 1F). At 8 h, 92.4% of wild-type cells showed a single Cen5-GFP focus, indicating that the Cen5 loci from the two homologs are closely paired. Among the *rad61/wpl1* mutant cells in the *ndt80* background, 70.0, 16.0, 7.9 and 6.0% contained one, two, three and four Cen5-GFP foci per cell (class I, II, III and VI), respectively (Figure 1G). This suggests a defect in SCC and a partial defect in homologous pairing in mid-prophase I in the *rad61/wpl1* mutant cells. These results suggest that Rad61/Wpl1 is a positive regulator of SCC and that it is required for efficient SCC and chromosome pairing.

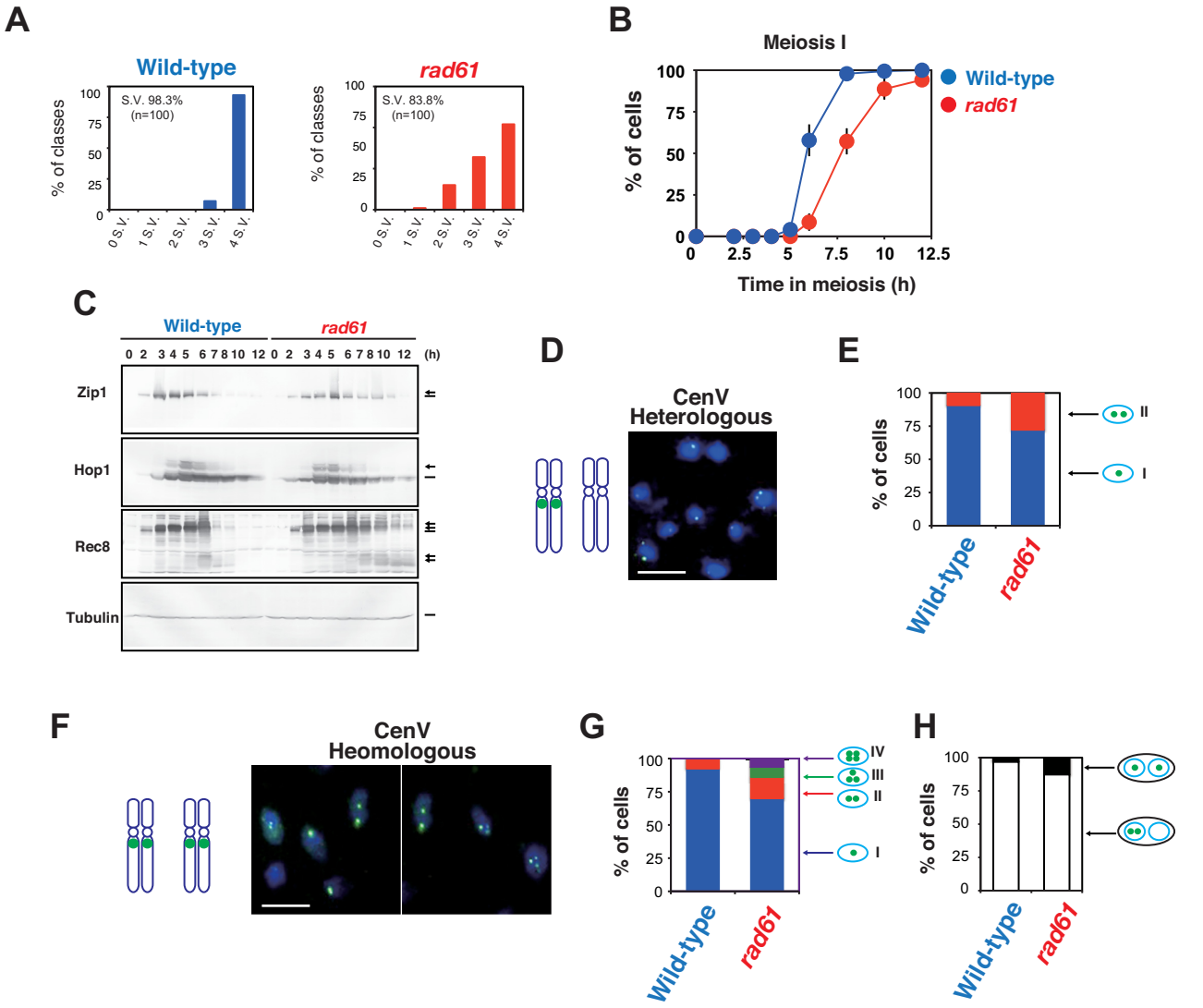

Figure 1. Rad61/Wpl1 is required for meiosis. (**A**) Distribution of viable spores per tetrad in various strains was measured and shown. Spores were incubated after dissection at 30°C for 3 days. Each bar indicates the percentage of classes with 4, 3, 2, 1 and 0 viable spores per tetrad. Spore viability and the total number of dissected tetrads (parentheses) are also shown. Wild-type (blue; MSY832/833) and *rad61/wpl1* (red; KSY63/64) cells. (**B**) Meiosis I was analyzed by DAPI staining of the wild-type (blue circles; MSY832/833) and *rad61/wpl1* (red circles; KSY63/64) cells. The number of DAPI bodies per nucleus was counted in a minimum of 150 DAPI positive cells at each time point. Plotted values represent the mean values with standard deviation (S.D.) from three independent experiments. (**C**) Expression of various meiotic proteins was verified by western blotting. At each time point, cells were fixed with trichloroacetic acid (TCA) and cell lysates were analyzed. Representative images are shown. The protein positions are indicated by the lines on the right. Phosphorylated species of Zip1, Hop1, and Rec8, as well as the cleaved Rec8 are shown by arrows. Wild-type, MSY832/833; *rad61/wpl1*, KSY63/64 cell lines were analyzed for protein expression. (**D** and **E**) Cohesion activity was monitored using a strain heterozygous for *CEN5-GFP*. GFP (green) and DAPI (blue) whole cell immunostaining was carried out. A representative image is shown (**D**). The number of cells with 1 (class I, blue) or 2 (class II, red) Cen5-GFP foci per cell was counted in a total of minimum 300 cells. The percentage of each class is shown as a graph on right. Cell lines that were analyzed are: *ndt80* (KSY391/405; $n = 318$), *rad61/wpl1 ndt80* (KSY447/449; $n = 299$). The bar indicates 2 μm. (**F**) Whole cell immunostaining using cells homozygous for *CEN5-GFP* (left) was carried out using GFP (green) and DAPI (blue) dyes. A representative image is shown on the right. The *ndt80* cells (KSY391/405; left); *rad61/wpl1 ndt80* cells (KSY447/449; right). The bar indicates 2 μm. (**G**) Homologous pairing was measured through the analyses of the number of Cen5-GFP foci per *ndt80* cell homozygous for *CEN5-GFP*: one foci indicates complete pairing (class I, blue); two foci indicates no pairing with normal cohesion or complete pairing with a cohesion defect for one sister pair (class II, red); three foci indicates no pairing with cohesion defect for one sister pair (class III, green); four foci indicates no paring with a full cohesion defect for two pairs of sister chromatids (class IV, purple). The *ndt80* cells (KSY404/405; $n = 437$); *rad61/wpl1 ndt80* cells (KSY448/449; $n = 531$). (**H**) Pattern of chromosome segregation in meiosis I was measured using a strain heterozygous for *CEN5-GFP*. Cells with two DAPI bodies were chosen and checked for the number of GFP dots in sister nuclei. When one sister nucleus contained two GFP spots, it was classified as 'reductional segregation (open)' On the other hand, a cell with two sister nuclei containing single GFP focus in each was classified as 'equational segregation (closed)'. Cell lines analyzed were: wild-type (KSY216/MSY833; $n = 132$), *rad61/wpl1* (KSY265/64; $n = 119$).

We also examined the effect of the *rad61/wpl1* deletion on chromosome segregation at meiosis I (Figure 1H). We used cells heterozygous for Cen5-GFP. We determined the fraction of cells with two DAPI-staining bodies that showed a GFP signal in only one of the two sister nuclei, the result expected if normal reductional segregation occurs as meiosis I. Wild-type cells showed 97% reductional chromosome segregation and only 3% contained a GFP signal in both of the two sister nuclei. The *rad61/wpl1* increased a frequency of equational segregation to 12.6% (chi-square test; $P = 4.0 \times 10^{-3}$). This indicates that Rad61/Wpl1 function is necessary for proper chromosome segregation in meiosis I.

Rad61/Wpl1 is necessary for proper meiotic recombination

As shown previously (15), a meiosis-specific α-kleisin Rec8 promotes the efficient formation and repair of meiotic DSBs. We investigated the role of Rad61/Wpl1 in the formation and repair of meiotic DSBs at the *HIS4-LEU2* recombination hotspot (39) (Figure 2A). The formation of DSBs at the *HIS4-LEU2* locus in the wild-type cells appeared at 3 h in meiosis, peaked at 4 h and thereafter gradually disappeared (Figure 2B and C; See also Figure 3D). The formation of DSBs in *rad61/wpl1* mutant cells was similar to that in wild-type cells, although maximal DSB formation was delayed, peaking at 5 h. The repair/loss of DSBs occurred at a slower rate than in wild-type cells, indicating that Rad61/Wpl1 is necessary for timely formation and efficient repair of DSBs.

To elucidate the role of Rad61/Wpl1 in meiotic recombination, immunostaining of two RecA homologs, Rad51 and Dmc1, that bind to ssDNA regions of DSBs (40,41) (Figure 2D) and that are markers for DSB repair during mitosis and meiosis (42,43) was conducted. Rad51/Dmc1 foci formed at 3 h, with levels peaking at 4 h before reaching background levels after 8 h of incubation in sporulation medium (Figure 2E). In the *rad61/wpl1* mutant, Rad51/Dmc1 foci form at 3 h, but their levels reached the maximum at 5 h, significantly later than in wild-types cells. The average number of Rad51 foci in the mutant was 37.8 ± 11.8 ($n = 48$) at 5 h, compared to 41.9 ± 11.1 ($n = 56$) at 4 h in wild-type cells. Thus, the number of Rad51 foci in the *rad61/wpl1* mutant was slightly decreased compared to that in the wild-type cells (Mann–Whitney *U*-test, $P = 3.6 \times 10^{-2}$). At 8 h, 28–30% of the mutant cells had persistent Rad51/Dmc1 foci (Figure 2D and E). These data are consistent with those obtained in experiments with *HIS4-LEU2,* suggesting that Rad61/Wpl1 controls efficient DSB formation and repair throughout the genome.

Meiotic cohesin complex is also required for the efficient formation of meiotic COs through its role in interhomolog bias (19). At *HIS4-LEU2* alleles, restriction polymorphisms between parental chromosomes produce DSBs, Joint-molecules (JMs) and recombination products (Figure 3A). One-dimensional gel (1D gel) analysis was used in order to quantify meiotic DSBs and COs/non-COs (NCO) (Figure 3B and D). In *rad61/wpl1* mutant cells, the turnover of DSBs is delayed compared with wild-type cells but ultimately disappears with about 1.5 h delay (Figure 3D). We examined the effect of the *rad61/wpl1* deletion on interhomolog bias by 2D gel analysis of the recombination intermediates at the *HIS4-LEU2* hotspot (19,35–36) (Figure 3A and C). This method can resolve three distinct branched DNA intermediates: Single-end invasions (SEIs), interhomolog double-Holliday junctions (IH-dHJs) and intersister dHJs (IS-dHJs). Physical analysis showed that the steady state levels of SEI were increased in the *rad61/wpl1* mutant cells compared with the wild-type cells (∼1.4-fold increase at 5 h in wild-type versus at 6 h in the mutant; Figure 3C and F). The disappearance of SEIs in the *rad61/wpl1* mutant cells was delayed ∼1.5 h relative to wild-type cells (Figure 3F). The formation of dHJs in the *rad61/wpl1* mutant cells showed ∼1 h delay relative to the wild-type cells (Figure 3E). Levels of IS-dHJs in the *rad61/wpl1* cells at 5 h were 1.3-fold higher than those in wild-type cells at 6 h (Figure 3H). Like IS-dHJs, IH-dHJs levels in the *rad61/wpl1* mutant cells at 6 h increased 1.4-fold compared with the levels in the wild-type cells at 4 h (Figure 3G). Thus, *rad61/wpl1* mutant cells showed similar interhomolog bias in comparison with the wild-type cells (Figure 3I). This suggests that Rad61/Wpl1 may promote efficient processing of intermediate in the interhomolog recombination.

We also analyzed CO and NCO recombination products (Figure 3B, bottom gel). Our findings are consistent with the previous reports that show that NCOs appear about 30 min earlier than COs at *HIS4-LEU2* locus in wild-type cells (44). Earlier appearance of NCO relative to CO is also seen in other recombination hotspots (45). However, in *rad61/wpl1* cells, COs and NCOs appeared at about the same time. Consistent with the turnover delay of JMs, the *rad61/wpl1* mutant cells also showed a delay in the formation of the recombination products. Moreover, both COs and NCOs in *rad61/wp1* mutants were decreased. The maximum levels of COs and NCOs in the mutant were reduced to 84 and 59% in the wild-type, respectively (Figure 3J and K). Furthermore, the *rad61/wpl1* strain had elevated CO to NCO ratio, such that NCOs were reduced in *rad61/wpl1* cells relative to wild-type cells (Figure 3L). These results suggest a role of Rad61/Wpl1 in the efficient NCO/CO differentiation.

It was previously shown that cohesin regulates DSB formation by modulation of axis structures (46). Particularly, cohesin promotes DSB formation on short chromosomes or on some regions of other chromosomes. We checked the effect of *rad61/wpl1* depletion on DSB formation. To measure steady state levels of DSBs, we analyzed DSB frequencies in the presence of the *rad50S* mutation, which blocks the processing of DSB ends (47). The *rad61/wpl1* mutant exhibited similar levels of DSBs at the *ARG4*, *BUD23* and *CYC1* loci (Supplemental Figure S1).

Chromosome morphogenesis is impaired in the *rad61/wpl1* mutant cells

In most organisms, chromosome pairing culminates in the development of chromosome synapsis, which is clearly manifested by the formation of the SCs (18). SC formation is tightly coupled with interhomolog recombination (48). As shown above, the *rad61/wpl1* mutant cells were partly deficient in homologous chromosome pairing and meiotic recombination. We also examined the role of Rad61/Wpl1 in SC formation, which was monitored by immunostaining

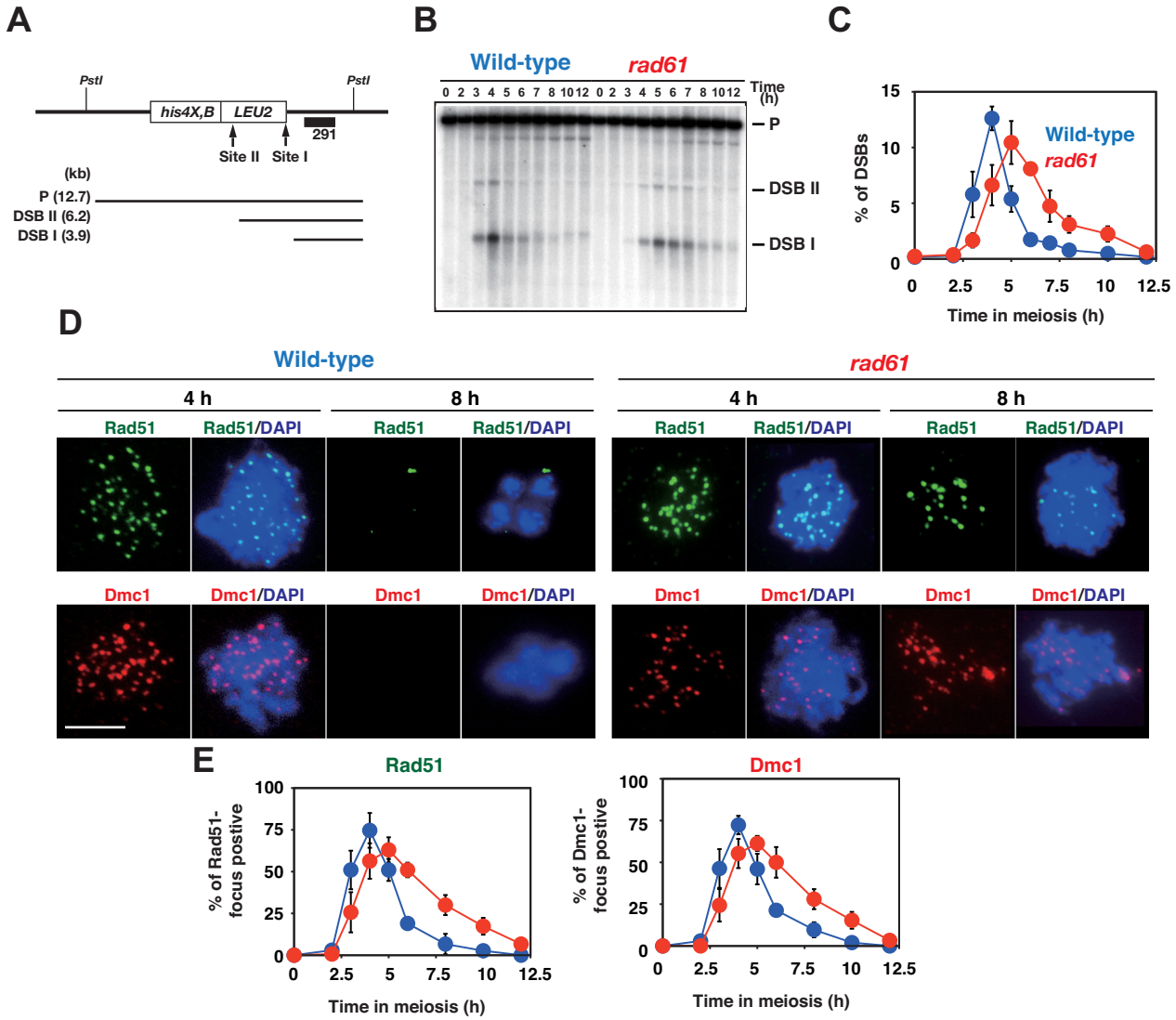

Figure 2. Rad61/Wpl1 promotes efficient recombination during meiosis. (**A**) Schematic representation of the *HIS4-LEU2* locus. Restriction enzyme sites and fragment sizes for double-strand breaks (DSB) and recombinant analyses are indicated with lines below. (**B**) DSB formation and repair at the *HIS4-LEU2* locus in the wild-type and *rad61/wpl1* strains were verified by Southern blotting. Genomic DNA was digested with PstI. (**C**) Kinetic analyses of meiotic DSBs. Parental and DSB bands were quantified and % of DSB was calculated. Graphs show the mean values with S.D. from three independent experiments. Wild-type cells (blue circles; NKY1303/1543) and *rad61/wpl1 cells* (red circles; KSY361/365). (**D**) Immunostaining analysis of Rad51 (green) and Dmc1 (red) in wild-type (NKY1303/1543) and *rad61/wpl1* (KSY361/365) mutant strains. Representative image with or without DAPI (blue) dye at 4 h for wild-type and 5 h for the *rad61/wpl1* is shown. The bar indicates 2 μm. (**E**) Kinetics of Rad51 (left) and Dmc1- (right) foci-positive cells in various yeast strains. A foci-positive cell is defined as a cell with more than five foci. A minimum of 100 cells were analyzed at each time point. Graphs show the mean values with S.D. from three independent experiments. The symbols represent the wild-type cells (blue circles; NKY1303/1543) and *rad61/wpl1* cells (KSY361/365).

analysis of Zip1 protein, a component of the central region of the SC (49). Zip1 staining in the wild-type cells (Figure 4A and Supplemental Figure S2A) was classified into three classes, dotty, partial linear and full linear staining, which correspond roughly to leptotene, zygotene and pachytene stages of meiosis prophase I, respectively. In wild-type cells, dotty staining of Zip1 peaked at 2 h, partial linear Zip1 was predominantly observed at 4 h and full SCs were seen at 5 h (Figure 4B). In the *rad61/wpl1* mutant cells, the appearance of Zip1 linear staining was slightly delayed in comparison with the wild-type cells. Cells with Zip1 dotty staining accumulated and peaked at 4 h in the mutant cells. This indicated a defect in SC elongation.

Immunostaining revealed shorter Zip1 lines in the *rad61/wpl1* mutant cells than in wild-type cells (Figure 4A). To study this in more detail, we investigated the loading of the components of the SC axial elements. In wild-type cells, Red1, a component of the SC lateral/axial elements (50), exhibited discontinuous immunostaining, in a way that some regions of the axes exhibited much stronger Red1 signals than others (Figure 4C and Supplemental Figure S2B). The immunostaining of *rad61/wpl1* mutant cells showed thicker and shorter Red1 lines of compared with those in the

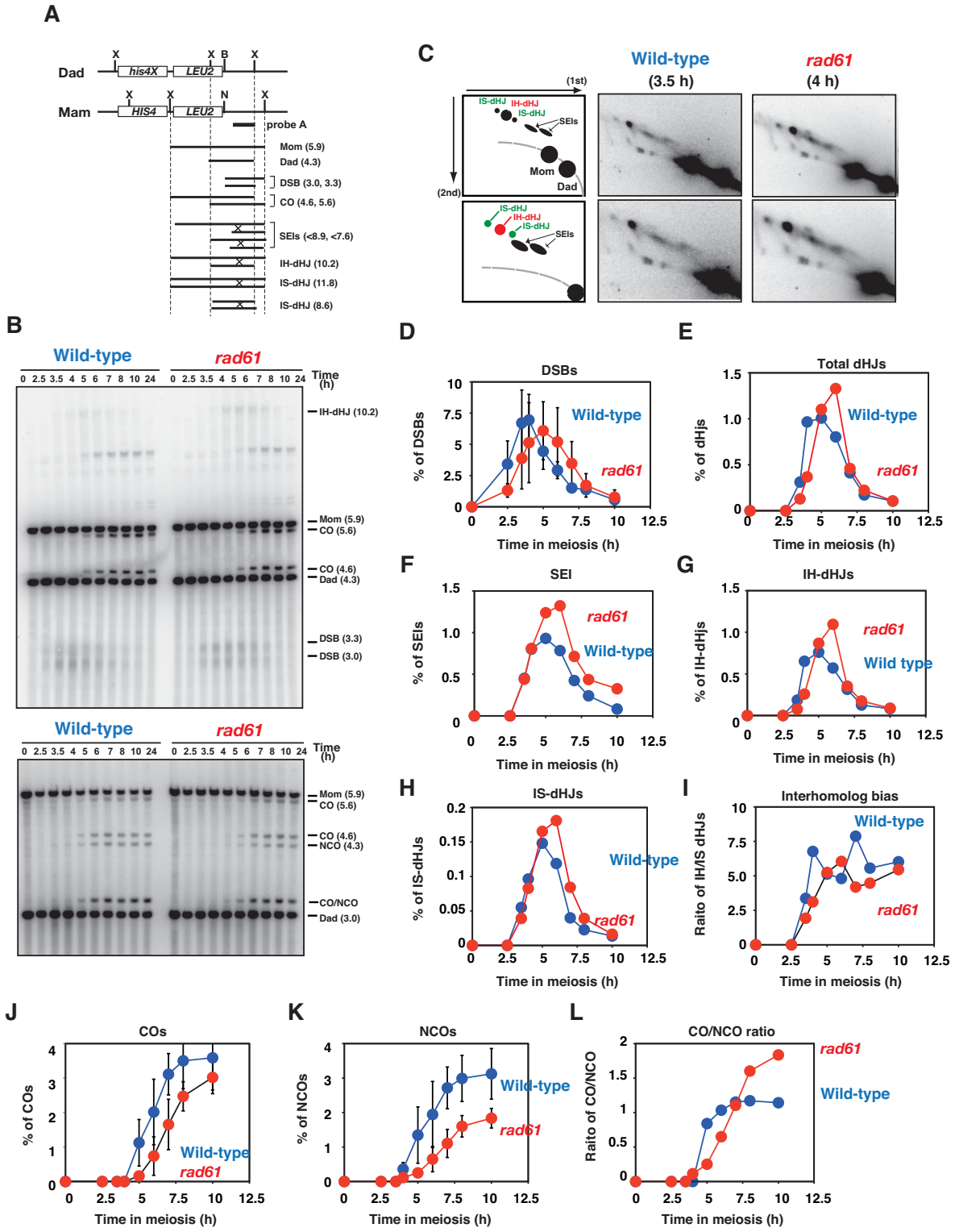

Figure 3. Rad61/Wpl1 promotes timely resolution of meiotic recombination intermediates. (**A**) Map of *HIS4LEU2* locus showing *Xho*I restriction sites, the position of Probe A, and DNA species generated by XhoI and NgoMIV digestion. DSBs, double-strand breaks; SEI, single-end invasion; IH-dHJ, interhomolog double-Holliday Junction; IS-dHJ, intersister double-Holliday Junction; CO, crossover. (**B**) One-dimensional (1D) gel analysis at *HIS4LEU2* locus in wild-type cells (KKY276) and *rad61/wpl1* cells (KKY1517). Top gel, *Xho*I-digested DNA species for DSB in panel **D**; Bottom gel, *Xho*I, *Ngo*MIV-double digested DNA for CO and non-crossover (NCO) in panels **J**–**L**. (**C**) Representative Southern blot images of the maximum level of JM species in wild-type (5 h) and *rad61/wpl1* (6 h) cells and schematic gel representations (left; bottom image is a magnified view of the top image). (D–L) Quantitation of DNA species shown in (**B** and **C**). The values shown are the means of two or three independent experiments. Wild-type cells, blue circles; *rad61/wpl1* cells, red circles. DSB kinetics ($n = 3$), **D**; dHJs (IH- and IS-dHJs) kinetics ($n = 2$), **E**; SEI, **F**; IH-dHJs ($n = 2$), G; IS-dHJs ($n = 2$), **H**; interhomolog ratio (IH-dHJs/IS-dHJs; $n = 2$), I; CO kinetics ($n = 3$), **J**; NCO kinetics ($n = 3$), **K**; CO/NCO ratio ($n = 3$), **L**.

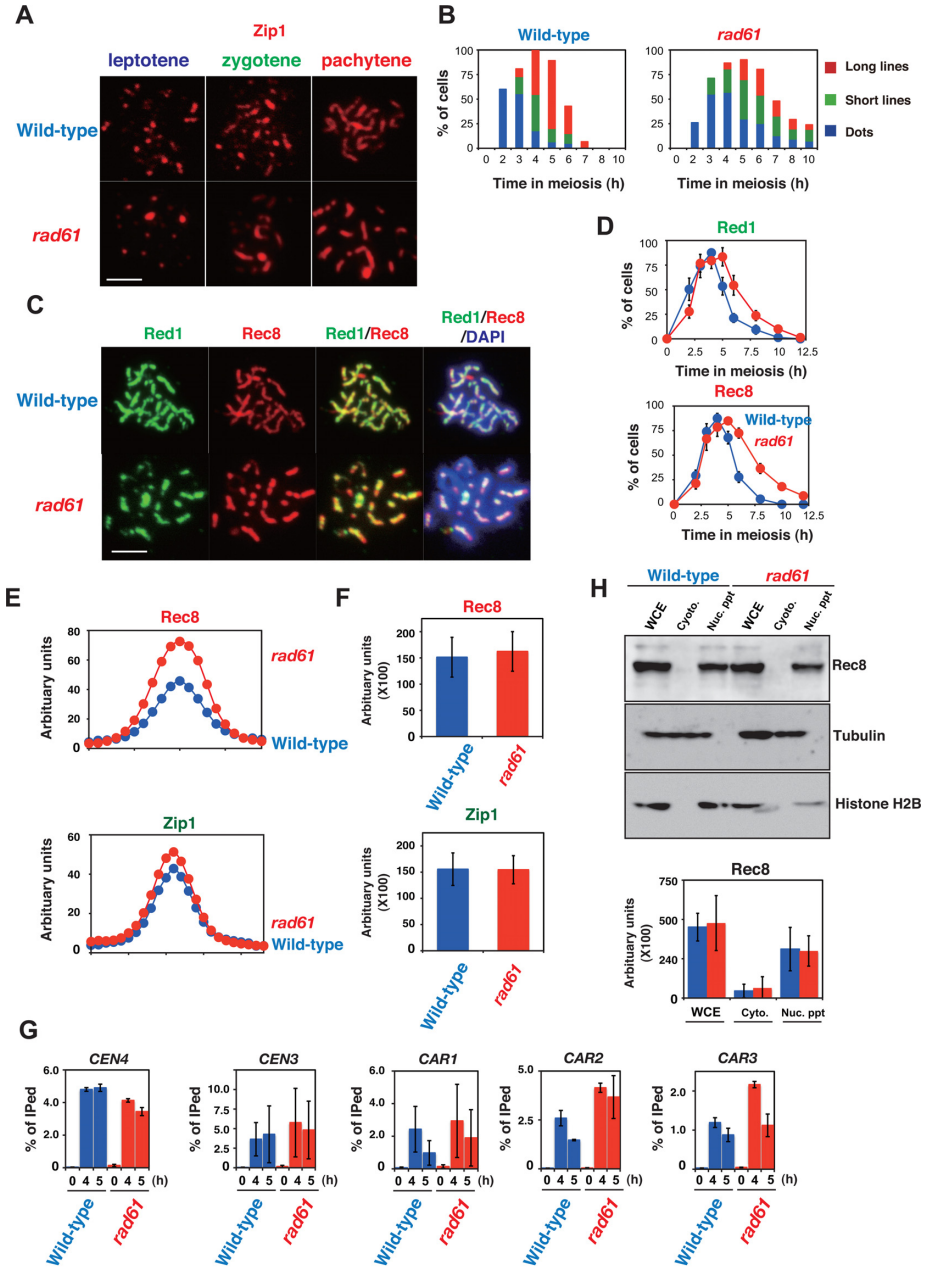

Figure 4. The *rad61/wpl1* mutant cells show hypercompaction of meiotic chromosomes. (**A**) Immunostaining analysis of a SC protein, Zip1 (**red**), was carried out in wild-type and mutant strains. Representative images are shown for each strain. Wild-type, MSY832/833; and *rad61/wpl1* (KSY63/64). The bar indicates 2 μm. Zip1 staining in the wild-type and mutant strains was classified as follows: dot (Class I, blue); partial linear (Class II, green); full SC (Class III, red). Spreads containing Zip1 lines were classified into two classes with <5 (class II, zygotene) and >5 (class III, pachytene) Zip1 foci/dots. (**B**) Kinetics of SC formation. Zip1 staining in wild-type and mutant strains was classified shown in (A).A minimum of 100 cells were analyzed per time point. Wild-type cells, MSY832/833*; rad61/wpl1* cells, KSY63/64. (**C**) Immunostaining analysis of chromosome proteins, Red1 (red) and Rec8 (green), was carried out in wild-type (MSY832/833) and the *rad61/wpl1* mutant (KSY63/64) strains. Representative images are shown for each strain. The bar indicates 2 μm. (**D**) Kinetics of chromosome spreads positive for Red1 (left) and Rec8 (right) were verified in wild-type and the *rad61/wpl1* strains. The symbols indicate the wild-type (blue circles; MSY832/833) and *rad61/wpl1* mutant (red circles; KSY63/64). Plotted values represent the mean values and S.D. from three independent experiments. (**E**) Line intensity analysis of Rec8 and Zip1 staining. Intensity of signal across lines was quantified as described in 'Materials and Methods' section. More than 30 lines on pachytene chromosome spreads were chosen and single intensity for Rec8 (top) and Zip1 (bottom) was measured. An average intensity is shown at each point of the line. The wild-type (blue circles; MSY832/833) and *rad61/wpl1* mutant (red circles; KSY63/64). (**F**) Total intensity of Rec8 (top) and Zip1 (bottom) lines per one pachytene nucleus was measured and means and S.D.s are shown. The wild-type (blue bars; $n = 24$) and *rad61/wpl1* mutant (red bars; $n = 29$) cells. (**G**) Chromatin immunoprecipitation (ChIP) analysis of Rec8 protein. ChIP for Rec8 was carried out and DNA molecules precipitated at 0, 4 and 5 h time points in meiosis of wild-type (blue; MSY832/833) and *rad61/wpl1* (red; KSY83/84) cells were analyzed by q-PCR. The percentage of precipitated DNA molecules compared with the total DNAs was calculated. A mean and S.D. from three independent experiments is shown. (**H**) Chromatin fractionation was carried out for Rec8, histone H2B and tubulin Whole cell extract (WCE) fractions of wild-type (blue; MSY832/833) and *rad61/wpl1* (red; KSY63/64) cells at 4 h, cytoplasm and chromatin were analyzed for the presence of Rec8 (top), tubulin (middle) and histone H2B (bottom). Relative intensities of Rec8 signals were calculated and shown as a graph. A mean and S.D. from three independent analyses is shown.

wild-type cells (Figure 4C). Red1 staining in the *rad61/wpl1* mutant cells was uniform relative to the wild-type cells which exhibited heterogeneous staining; e.g. beads-in-line. Assembly and disassembly of Red1 on chromosomes were slightly delayed in the *rad61/wpl1* mutant cells compared with the wild-type cells (Figure 4D). These results suggest that Rad61/Wpl1 promotes formation of properly assembled chromosome axes.

The possible shortening of SC, and consequently chromosomes, was further confirmed by Rec8 staining. This staining also showed discontinuous lines on SCs in the wild-type cells (15) (Figure 4C; Supplemental Figure S3B). Moreover, the *rad61/wpl1* mutant cells were proficient in the loading of Rec8 on meiotic chromosomes. Kinetic analysis indicated normal assembly and delayed disassembly of Rec8 from meiotic chromosomes (Figure 4D). Notably, Rec8-immunostained lines in the *rad61/wpl1* mutant cells were thicker and shorter than those in the wild-type cells, suggesting that Rad61/Wpl1 controls chromosome compaction during meiosis.

Chromosome axes are shortened in the *rad61/wpl1* mutant cells

The data we present here suggest that the *rad61/wpl1* mutation induces the shortening of chromosome axes. We measured the physical distance between a centromere (*TRP1*) and a telomere on the right arm of chromosome IV, both of which were marked with LacI-GFP (∼1.05 Mbp; heterozygous for the LacI-GFP; Figure 5A) (51). Double staining for LacI-GFP and Rec8 revealed two LacI-GFP foci. At 0 h (which corresponds to the mitotic G1 cell phase), the average distance between the investigated loci in the wild-type cells was 1.60 ± 0.46 μm. (Figure 5A and B; $n = 45$). The distance in *rad61/wpl1* mutant cells was 1.51 ± 0.46 μm, which was not significantly different from the average distance in wild-type cells (Student's *t*-test, $P = 0.378$). Compacted chromosomes have been reported previously in the ribosomal DNA (rDNA) locus of the *rad61/wpl1* mutant cells during mitosis (52,53). We measured the distance between two GFP loci in meiosis. At 4 h, when most of cells were in zygotene/pachytene, in wild-type cells the distance was reduced to 1.17 ± 0.35 μm (compared with the distance at 0 h; $P = 2.7 \times 10^{-6}$) (Figure 5A and B), indicating shortening of the chromosome axis during meiotic prophase I. The average length between the loci in the *rad61/wpl1* mutant cells at 4 h was 0.75 ± 0.25 μm. (*t*-test, versus the wild-type at 4 h, $P = 2.0 \times 10^{-9}$), indicating shortening of chromosomes in the mutant cells relative to the wild-type cells.

We also analyzed the distance between two LacI-GFP loci in a single cell (Figure 5C). Distances between GFP signals were measured after generating a set of serial images of each cell in different focal planes and then collapsing the image stack to create a single 2D image (Figure 5C and D). At 0 h, in the wild-type and the *rad61/wpl1* mutant cells we measured the distances of 1.61 ± 0.50 and 1.36 ± 0.48 μm ($n = 155$) between the two foci, respectively. The results of this assay indicate shortening of the distance between the two chromosomal loci in mitotic G1 *rad61/wpl1* cells ($P = 1.5 \times 10^{-5}$). At 4 h, in meiotic prophase I, the distance in wild-type and the *rad61/wpl1* mutant cells was 1.34 ± 0.40 and 0.78 ± 0.23 μm, respectively ($P = 5.6 \times 10^{-3}$). Again, shortening of the chromosome occurs during the wild-type meiosis, while the *rad61/wpl1* mutant shows increased chromosome compaction during both meiosis and mitosis.

The *rad61/wpl1* mutant cells show wild-type Rec8 levels on chromosomes

Previously, the *Schizosaccharomyces pombe pds5* deletion mutant showed the compaction of the axes with reduced Rec8 binding to chromosomes (54), while meiosis-specific *S. cerevisiae PDS5* depletion mutant showed the shortened axes, but normal Rec8 binding (24). We checked the amount of Rec8 on chromosomes using three different methods. First, we quantified line intensity of immunostained Rec8 as well as Zip1 signals on a pachytene chromosome (Figure 4C). This allowed a comparison of the signal intensity on axial elements with the signal intensity of the central element (Figure 4E). Average peak intensity of Rec8 in the *rad61/wpl1* mutant is 1.58× brighter than in the wild-type cells. Zip1 shows narrower signal distribution than Rec8. The *rad61/wpl1* cells showed 1.20× brighter Zip1 peak than the wild-type cells. Given that the Rec8 signal intensity was compensated by the compaction ratio (1.56 in Figure 5B), the ratio should be 1.01 (1/58/1.56), indicating a normal amount of Rec8 in the absence of Rad61/Wpl1. Indeed, when we measured the total intensities of Rec8 or Zip1 signal per nucleus, average intensities of Rec8 and Zip1 were not different between the wild-type and *rad61/wpl1* cells (Figure 4F; Zip1 signal in the wild-type cells is often discontinuous). Second, we also examined Rec8 binding to chromosomal loci by ChIP. As previously reported (24), Rec8 binds to centromeres (*CEN3* and *CEN4*) as well as chromosomal loci such as cohesin association region (CARC; *CARC1*, *−2* and *−3*) at 4 and 5 h, but not at 0 h in wild-type cells (Figure 4G). Rec8-binding at 4 or 5 h in the *rad61/wpl1* mutant cells was similar to that in the wild-types. This shows that the amount of Rec8 on chromosomes is similar in wild-type and *rad61/wpl1* mutant. Furthermore, we checked the amount of Rec8 protein in a fraction of chromatin pellets (Figure 4H). Quantification of Rec8 showed that the amount of Rec8 was indistinguishable between the wild-type and the *rad61/wpl1* mutant cells. These three experiments strongly support the notion that the *rad61/wpl1* mutation does not affect the Rec8 amount on meiotic chromosomes.

Rad61/Wpl1 regulates timely disassembly of chromosome bouquets

Previous studies have shown that the Rec8 cohesin complex controls the telomere dynamics in meiotic cells (55,56). During meiosis, telomeres bound to the nuclear envelop (NE) occasionally form a large cluster, the telomere bouquet (57). Telomere dynamics can be monitored using a GFP-tagged telomere binding protein Rap1 (21). In mitotic cells, several Rap1-GFP foci were observed on a single focal plane of the nuclei (Figure 6A). During meiotic prophase I, the number of Rap1-GFP foci increased and these foci formed a cluster in one region of cell nuclei (arrows in Figure 6A). This Rap1-GFP clustering was transient in wild-type cells (57).

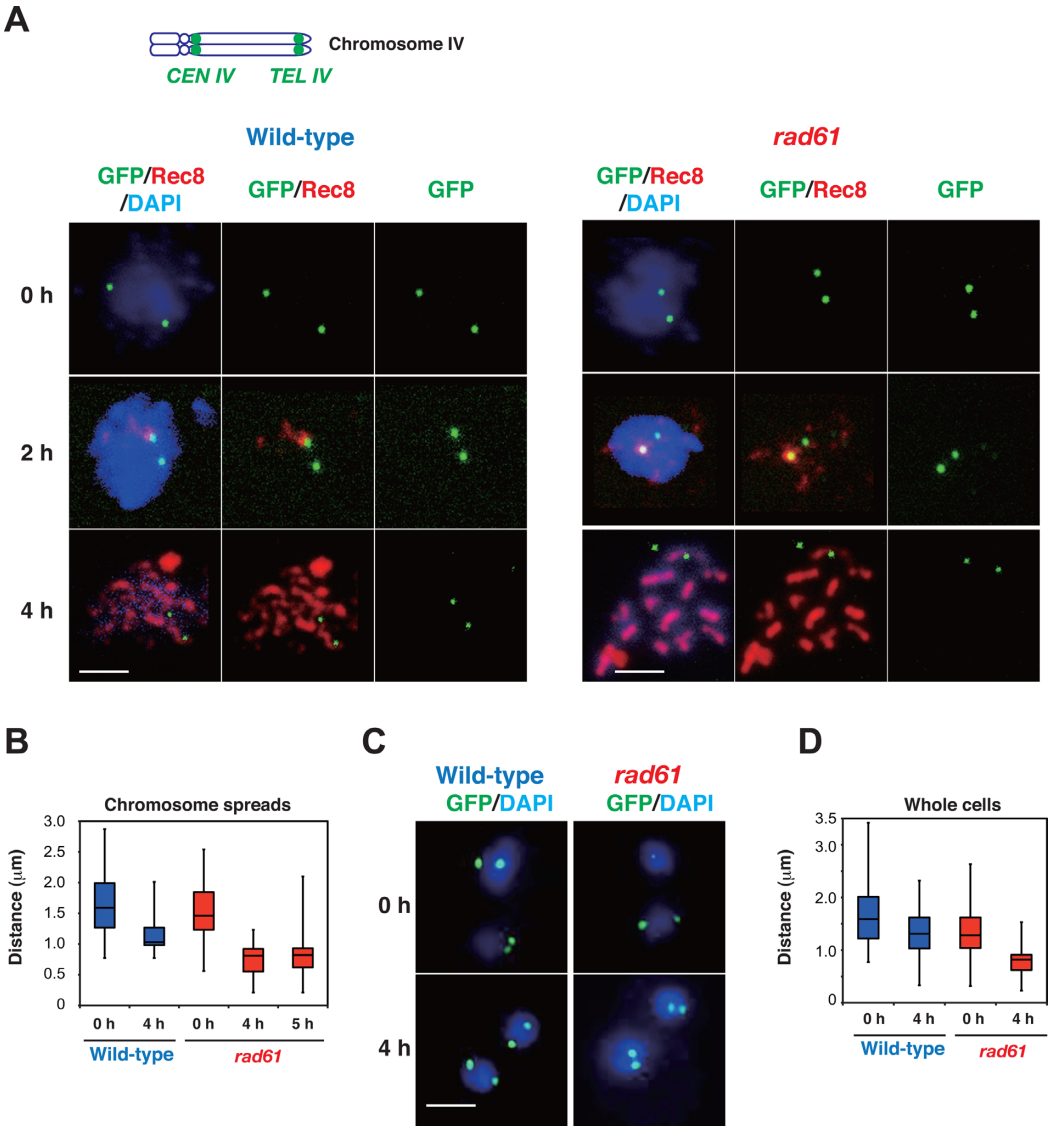

Figure 5. The *rad61/wpl1* mutant strain shows hypercompaction of meiotic chromosomes. (**A**) The distances between two *CEN4* and *TEL4* GFP foci (above) were measured for each strain. Representative images of GFP foci (green), Rec8 (red) and DNA (blue) in wild-type (KSY315/MSY833), and the *rad61/wpl1* (KSY343/64) cells on chromosome spreads at each time point is shown. The bar indicates 2 μm. (**B**) The distances between *CEN4* (*TRP1*, right) and *TEL4* (left) at each time point (0, 2 and 4 h) were measured and plotted as box and whisker plots. For chromosome spreads, the distances were measured in 45 samples with pachytene staining of Rec8. Wild-type cells, blue; *rad61/wpl1* cells. (**C**) Representative images of *CEN4* and *TEL4* GFP foci (green) and nuclei (blue) in wild-type (KSY315/MSY833) and the *rad61/wpl1* (KSY343/64) cells in a single focal plane of whole cell staining at each time point is shown. The bar indicates 2 μm. (**D**) Distances between *CEN4* (right) and *TEL4* (left) at each time point (0 and 4 h) were measured and plotted as a box and whisker plot. For whole cell imaging, the distance was analyzed in 155 samples. Wild-type cells, blue; *rad61/wpl1* cells, red.

A fraction of cells containing Rap1-GFP cluster was seen at 2 h and 3 h in wild-type cells with a frequency of 25.0 ± 4.0 and 28.3 ± 1.5%, respectively (Figure 6B). On the other hand, the *rad61/wpl1* mutant cells gradually accumulated the Rap1-GFP clusters at a frequency of 47 ± 6.7% at 5 h. At 6 h, the telomere clustering was resolved in the mutant cells. The *rec8* mutant cells showed persistent Rap1-GFP clustering during the prophase I (56). These results indicate that Rad61/Wpl1 positively regulates telomere dynamics.

The telomere dynamics on NE during meiosis in budding yeast are promoted by Mps3 (55,58). Mps3 is a SUN(Sad1-Unc-84)-domain protein that localizes to the inner nuclear membrane (55). We analyzed the localization of Mps3 on the NE using Mps3-GFP fusion protein. As shown previously in vegetative cells (e.g. at 0 h) (55,58), Mps3-GFP showed a single focus corresponding to the spindle pole body (SPB; Figure 6C). Once cells entered meiosis, Mps3-GFP showed different distributions on the NE. In early meiosis I (at 2 h), we observed a reduced number of Mps3-GFP (≤5 foci). Larger Mps3-GFP foci or patches appeared before the transient clustering of Mps3-GFP foci was seen at 3 h, with a frequency of 18.7 ± 2.3% (Figure 6D). This Mps3-GFP clustering was resolved during further incubation. The numbers of foci/patches containing Mps3-GFP on NE increased during incubation, until the late prophase I. Afterward, at 5–6 h, Mps3-GFP molecules were seen on

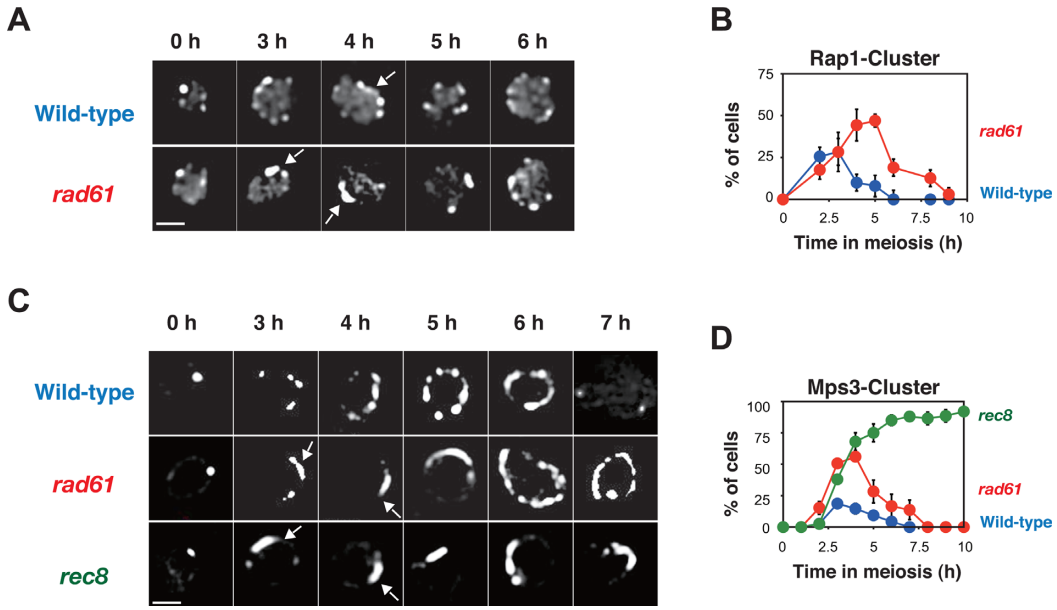

Figure 6. Rad61/Wpl1 promotes efficient telomere dynamics in prophase I. (**A**) Telomere dynamics was monitored in meiotic cells with Rap1-GFP. A representative image of each time point in wild-type (KSY61/62) and *rad61/wpl1* (KSY123/124) cells is shown. The bar indicates 2 μm. (**B**) Kinetics of telomere clustering was examined in meiotic cells with Rap1-GFP staining. At each time point, cells with a large Rap1-GFP cluster were counted ($n = 100$). Plotted values represent the mean ±S.D., from three independent experiments. Wild-type (KSY61/62) cells, blue circles; *rad61/wpl1* (KSY123/124) cells, red circles. (**C**) Mps3-GFP dynamics was monitored in meiotic cells. A representative image of each time point for three different strains, wild-type (KSY97/98), *rad61/wpl1* (KSY42/43) and *rec8* (KSY271/272) cells is shown. (**D**) Percentage of the cells with a cluster of Mps3 foci/patches was measured and plotted over time in meiosis. Plotted values represent the mean and S.D. from three independent experiments. Wild-type (KSY97/98), blue; *rad61/wpl1* (KSY42/43), red; *rec8* (KYS271/272), green. The *rec8* mutant shows persistent clustering of Mps3.

most of the NE. When cells exited prophase I, Mps3-GFP signals on the NE disappeared, leaving two foci on the duplicated SPBs. The *rad61/wpl1* mutant showed altered kinetics of Mps3-GFP dynamics with an increased Mps3-GFP clustering of 56.0 ± 2.0% at 4 h, and this clustering was resolved later in comparison with the wild-type cells. However, as it was shown previously (55), the *rec8* mutant cells accumulated Mps3-GFP clustering without any resolution. The *rad61/wpl1* mutant partially recapitulates the defect in telomere clustering resolution seen in the *rec8* mutant. These results demonstrate that Rad61/Wpl1 positively controls Mps3 dynamics as the Rec8–cohesin complex, and consequently chromosome dynamics during meiosis.

DISCUSSION

In addition to its role in SCC, the cohesin complex plays multiple different roles in meiotic chromosome dynamics. Rad61/Wpl1 (Wapl), a non-essential subunit of the cohesin, is known to be a negative regulator of the cohesin complex (9–11). In this study, we have demonstrated that Rad61/Wpl1 controls chromosome compaction as well as meiotic chromosome dynamics and in particular the events occurring at zygotene/pachytene transition; e.g. SEI/dHJ transition and resolution of telomere clustering.

Rad61/Wpl1 controls chromosome axis compaction

In the *rad61/wpl1* mutant cells, the length of SC was seen to be reduced in comparison with the length in the wild-type cells, possibly as a result of the shortening of the axes. Consistent with this, uniform Rec8 staining was seen in the mutant cells, compared with the discontinuous staining observed in the wild-type cells. We confirmed that the distance between two chromosomal loci on a single chromosome is reduced in the *rad61/wpl1* mutant cells, and this confirmed that chromosome axes are shorter in the mutant cells. This suggests a role of Rad61/Wpl1, and therefore a role of Rec8 and the cohesin complex, in the morphogenesis of chromosome axes. The shortening of axes in *rad61/wpl1* mutant cells may be associated with the formation of chromatin loops longer than those in the wild-type cells. Alternatively, this shortening may be due to the much tighter compaction without the alteration of loop sizes. The number of chromosome-associated Rec8 proteins does not differ between wild-type and *rad61/wpl1* cells. This is consistent with the latter possibility. It is likely that Rad61/Wpl1 is able to regulate three-dimensional architecture of chromosome axes containing the cohesin, without affecting its loading. However, the measurements of the axis-associated chromatin loop size are still needed.

Axis compaction of meiotic chromosomes without the reduction of Rec8 binding is also reported for the budding yeast *pds5* depletion mutant (24), suggesting that Rad61/Wpl1 controls meiotic axis compaction with Pds5. However, the *rad61/wpl1* mutant cells form SC between homologous chromosomes, while the *pds5* depletion mutant cells induce SC formation between sister chromatids (24), indicating different roles of Rad61/Wpl1 and Pds5 proteins in the cohesin-mediated chromosome synapsis in meiosis. SC shortening, and consequently axis compaction, was also observed in mice lacking Smc1β, a meiosis-specific Smc1

isoform (59). Additionally, the *pds5* deletion mutant in the fission yeast showed more compact Rec8 staining of meiotic chromosomes, with decreased Rec8-binding to chromosomes (54). Based on these studies, the change in cohesin architecture along chromatin might regulate the extension and/or compaction of chromosome axes. In *Caenorhabditis elegans*, mutants lacking the Wapl homologues (*wapl-1*) also display shortening axial elements during meiotic prophase (E. Martinez-Perez, personal communication). This supports the idea that the cohesin complex is a critical determinant of the meiotic chromosomal axis compaction.

As described previously, meiotic chromosomes in the wild-type cells contain Rec8-rich and Rec8-poor regions (20,46,60). Rad61/Wpl1 may promote the formation of Rec8-poor regions on the chromosomes through the negative regulation of the local dynamics of Rec8 with some compensatory effect on Rec8-rich region. This is supported by a Rad61/Wpl1 role in the promotion of the cohesin molecule dissociation (9–11), i.e. Rad61/Wpl1 might facilitate the context-dependent dissociation of Rec8-cohesin. Furthermore, some chromosomal regions may have a greater ability to suppress Rad61/Wpl1 activity than other regions. It is shown that the acetylation of Smc3 by Eco1 promotes the stable association of cohesin to chromosomes, by counteracting the activities of Rad61/Wpl1 and Pds5 (8,10–11,61). It was shown previously that Eco1 is recruited to DSBs in order to facilitate a stable association of the cohesin with DSB sites during mitosis (8,61). Meiotic DSBs may also trigger the acetylation of Smc3, which may contribute to different stability of the complex in the distinct chromosomal regions. Without Rad61/Wpl1, these region-specific differences might be inhibited, resulting in the uniform loading of Rec8 cohesin to chromosomes and axis shortening.

Rad61/Wpl1 promotes meiotic recombination

We found that the *rad61/wpl1* mutant cells show distinct defects in meiotic recombination. First, Rad61/Wpl1 promotes timely formation of meiotic DSBs. This is supported by a delayed loading of Rad51/Dmc1 on meiotic chromosomes, as well as a delayed formation of the DSBs at the *HIS4-LEU2* recombination hotspot in the *rad61/wpl1* mutant cells. Given that Rec8 is necessary for efficient and timely DSB formation (15), this suggests that Rad61/Wpl1 also positively regulates DSB formation, although it is not involved in the regulation of DSB formation frequencies in the *rad50S* background (Supplemental Figure S2). Alternatively, this might be simply due to delay in DSB processing in this mutant since it is recently shown that DSBs tend to form if the processing of recombination mediates are delayed (62,63). Next, our results demonstrate that Rad61/Wpl1 is needed for the efficient DSB repair, whose defect might induce delay in prophase I. Cohesin is known to promote DSB repair between sister chromatids in mitotic cells (64). These results also confirm that Rad61/Wpl1 seems to stimulate the activity of this complex in DSB repair. Finally, the *rad61/wpl1* mutant cells decrease NCOs at the *HIS4-LEU2* hotspot more than COs and increase NCO at some loci. Given that the NCO formation is mediated by an early-branched recombination pathway (35,45), Rad61/Wpl1, and consequently cohesin, controls CO formation, through the control of CO/NCO decision. Taken together, these data reveal a positive role of Rad61/Wpl1 as a component of the cohesin complex in processing of the recombination intermediates.

Rad61/Wpl1 promotes telomere dynamics

Previous studies showed that Rec8 regulates chromosome dynamics during meiotic prophase I (56). However, it is not clear whether Rec8 is involved in this role through the cohesin complex or through a telomere complex with Rec8. The results described in this study show that not only Rec8, but also its regulator Rad61/Wpl1, are necessary for the efficient telomere dynamics during meiosis, supporting the conclusion that Rec8 as a part of the cohesin complex controls the dynamics of meiotic telomeres. The movements of telomeres in meiotic cells are mediated by a telomere/NE ensemble, which includes a SUN protein Mps3 (65). This suggests that Rec8-cohesin promotes the resolution of telomeres by affecting the function of Mps3 on NE ensembles through the change of either global chromosome structure or telomeric chromatin structure.

SUPPLEMENTARY DATA

Supplementary Data are available at NAR Online.

ACKNOWLEDGEMENTS

We are grateful to Drs N. Hunter and H. B. D. P. Rao as well as the members of the Shinohara lab for helpful discussions and Ms A. Murakami and S. Umetani for excellent technical assistance. We are grateful to Drs K. Nasmyth and D. Koshland for materials used in this study and to Dr E. Martinez-Perez for the personal communication on *wpl-1* in nematodes.
Authors: K.C., M.S. and A. S. designed the experiments. K.C., M.S., M.L. and K.K. performed the experiments and analyzed the data. K.C., M.S., K. K. and A.S. prepared the manuscript.

FUNDING

JSPS KAKENHI [22125001, 22125002 to A.S.]; Asahi-Glass Science Foundation (to A.S.); Uehara Science Foundation (to A.S.); Mochida Medical Science Foundation (to A.S.); Takeda Science Foundation (to A.S.); Japan Society for the Promotion of Science (JSPS) through the Funding Program for Next Generation World-Leading Researchers (NEXT Program) (to M.S.); National Research Foundation of Korea (NRF) grant funded by the Government of Korea (MSIP) [No. 2014R1A2A1A11051584 to K.P.K.]. Funding for open access charge: A Grant-in-Aid from the Ministry of Education, Science, Sport and Culture, JAPAN.
Conflict of interest statement. None declared.

REFERENCES

1. Marston,A.L. (2014) Chromosome segregation in budding yeast: sister chromatid cohesion and related mechanisms. *Genetics*, **196**, 31–63.

2. Remeseiro,S. and Losada,A. (2013) Cohesin, a chromatin engagement ring. *Curr. Opin. Cell Biol.*, **25**, 63–71.
3. Gruber,S., Haering,C.H. and Nasmyth,K. (2003) Chromosomal cohesin forms a ring. *Cell*, **112**, 765–777.
4. Huang,C.E., Milutinovich,M. and Koshland,D. (2005) Rings, bracelet or snaps: fashionable alternatives for Smc complexes. *Philos. Trans. R. Soc. Lond. B Biol. Sci.*, **360**, 537–542.
5. Uhlmann,F., Lottspeich,F. and Nasmyth,K. (1999) Sister-chromatid separation at anaphase onset is promoted by cleavage of the cohesin subunit Scc1. *Nature*, **400**, 37–42.
6. Shirayama,M., Toth,A., Galova,M. and Nasmyth,K. (1999) APC(Cdc20) promotes exit from mitosis by destroying the anaphase inhibitor Pds1 and cyclin Clb5. *Nature*, **402**, 203–207.
7. Rolef Ben-Shahar,T., Heeger,S., Lehane,C., East,P., Flynn,H., Skehel,M. and Uhlmann,F. (2008) Eco1-dependent cohesin acetylation during establishment of sister chromatid cohesion. *Science*, **321**, 563–566.
8. Unal,E., Heidinger-Pauli,J.M., Kim,W., Guacci,V., Onn,I., Gygi,S.P. and Koshland,D.E. (2008) A molecular determinant for the establishment of sister chromatid cohesion. *Science*, **321**, 566–569.
9. Kueng,S., Hegemann,B., Peters,B.H., Lipp,J.J., Schleiffer,A., Mechtler,K. and Peters,J.M. (2006) Wapl controls the dynamic association of cohesin with chromatin. *Cell*, **127**, 955–967.
10. Rowland,B.D., Roig,M.B., Nishino,T., Kurze,A., Uluocak,P., Mishra,A., Beckouet,F., Underwood,P., Metson,J., Imre,R. *et al.* (2009) Building sister chromatid cohesion: Smc3 acetylation counteracts an antiestablishment activity. *Mol. Cell*, **33**, 763–774.
11. Sutani,T., Kawaguchi,T., Kanno,R., Itoh,T. and Shirahige,K. (2009) Budding yeast Wpl1(Rad61)-Pds5 complex counteracts sister chromatid cohesion-establishing reaction. *Curr. Biol.*, **19**, 492–497.
12. Petronczki,M., Siomos,M.F. and Nasmyth,K. (2003) Un menage a quatre: the molecular biology of chromosome segregation in meiosis. *Cell*, **112**, 423–440.
13. Kitajima,T.S., Kawashima,S.A. and Watanabe,Y. (2004) The conserved kinetochore protein shugoshin protects centromeric cohesion during meiosis. *Nature*, **427**, 510–517.
14. Haering,C.H. and Jessberger,R. (2012) Cohesin in determining chromosome architecture. *Exp. Cell Res.*, **318**, 1386–1393.
15. Klein,F., Mahr,P., Galova,M., Buonomo,S.B., Michaelis,C., Nairz,K. and Nasmyth,K. (1999) A central role for cohesins in sister chromatid cohesion, formation of axial elements, and recombination during yeast meiosis. *Cell*, **98**, 91–103.
16. Ishiguro,K., Kim,J., Fujiyama-Nakamura,S., Kato,S. and Watanabe,Y. (2011) A new meiosis-specific cohesin complex implicated in the cohesin code for homologous pairing. *EMBO Rep.*, **12**, 267–275.
17. Lee,J. and Hirano,T. (2011) RAD21L, a novel cohesin subunit implicated in linking homologous chromosomes in mammalian meiosis. *J. Cell Biol.*, **192**, 263–276.
18. Zickler,D. and Kleckner,N. (1999) Meiotic chromosomes: integrating structure and function. *Annu. Rev. Genet.*, **33**, 603–754.
19. Kim,K.P., Weiner,B.M., Zhang,L., Jordan,A., Dekker,J. and Kleckner,N. (2010) Sister cohesion and structural axis components mediate homolog bias of meiotic recombination. *Cell*, **143**, 924–937.
20. Kugou,K., Fukuda,T., Yamada,S., Ito,M., Sasanuma,H., Mori,S., Katou,Y., Itoh,T., Matsumoto,K., Shibata,T. *et al.* (2009) Rec8 guides canonical Spo11 distribution along yeast meiotic chromosomes. *Mol. Biol. Cell*, **20**, 3064–3076.
21. Hayashi,A., Ogawa,H., Kohno,K., Gasser,S.M. and Hiraoka,Y. (1998) Meiotic behaviours of chromosomes and microtubules in budding yeast: relocalization of centromeres and telomeres during meiotic prophase. *Genes Cells*, **3**, 587–601.
22. Rao,H.B.D.P., Shinohara,M. and Shinohara,A. (2011) Mps3 SUN domain-dependent chromosome motion controls juxtaposition of homologous chromosomes during meiosis. *Genes Cells*, **16**, 1081–1096.
23. Michaelis,C., Ciosk,R. and Nasmyth,K. (1997) Cohesins: chromosomal proteins that prevent premature separation of sister chromatids. *Cell*, **91**, 35–45.
24. Jin,H., Guacci,V. and Yu,H.G. (2009) Pds5 is required for homologue pairing and inhibits synapsis of sister chromatids during yeast meiosis. *J. Cell Biol.*, **186**, 713–725.
25. De Antoni,A. and Gallwitz,D. (2000) A novel multi-purpose cassette for repeated integrative epitope tagging of genes in *Saccharomyces cerevisiae*. *Gene*, **246**, 179–185.
26. Shinohara,M., Gasior,S.L., Bishop,D.K. and Shinohara,A. (2000) Tid1/Rdh54 promotes colocalization of Rad51 and Dmc1 during meiotic recombination. *Proc. Natl. Acad. Sci. U.S.A.*, **97**, 10814–10819.
27. Shinohara,M., Oh,S.D., Hunter,N. and Shinohara,A. (2008) Crossover assurance and crossover interference are distinctly regulated by the ZMM proteins during yeast meiosis. *Nat. Genet.*, **40**, 299–309.
28. Zhu,Z., Mori,S., Oshiumi,H., Matsuzaki,K., Shinohara,M. and Shinohara,A. (2011) Cyclin-dependent kinase promotes formation of the synaptonemal complex in yeast meiosis. *Genes Cells*, **15**, 1036–1050.
29. Shinohara,M., Sakai,K., Ogawa,T. and Shinohara,A. (2003) The mitotic DNA damage checkpoint proteins Rad17 and Rad24 are required for repair of double-strand breaks during meiosis in yeast. *Genetics*, **164**, 855–865.
30. Sasanuma,H., Tawaramoto,M.S., Lao,J.P., Hosaka,H., Sanda,E., Suzuki,M., Yamashita,E., Hunter,N., Shinohara,M., Nakagawa,A. *et al.* (2013) A new protein complex promoting the assembly of Rad51 filaments. *Nat. Commun.*, **4**, 1676.
31. Hayase,A., Takagi,M., Miyazaki,T., Oshiumi,H., Shinohara,M. and Shinohara,A. (2004) A protein complex containing Mei5 and Sae3 promotes the assembly of the meiosis-specific RecA homolog Dmc1. *Cell*, **119**, 927–940.
32. Kee,K., Protacio,R.U., Arora,C. and Keeney,S. (2004) Spatial organization and dynamics of the association of Rec102 and Rec104 with meiotic chromosomes. *EMBO J.*, **23**, 1815–1824.
33. Bani Ismail,M., Shinohara,M. and Shinohara,A. (2014) Dot1-dependent histone H3K79 methylation promotes the formation of meiotic double-strand breaks in the absence of histone H3K4 methylation in budding yeast. *PLoS One*, **9**, e96648.
34. Shinohara,A., Gasior,S., Ogawa,T., Kleckner,N. and Bishop,D.K. (1997) *Saccharomyces cerevisiae recA* homologues *RAD51* and *DMC1* have both distinct and overlapping roles in meiotic recombination. *Genes Cells*, **2**, 615–629.
35. Hunter,N. and Kleckner,N. (2001) The single-end invasion: an asymmetric intermediate at the double-strand break to double-holliday junction transition of meiotic recombination. *Cell*, **106**, 59–70.
36. Schwacha,A. and Kleckner,N. (1994) Identification of joint molecules that form frequently between homologs but rarely between sister chromatids during yeast meiosis. *Cell*, **76**, 51–63.
37. Game,J.C., Birrell,G.W., Brown,J.A., Shibata,T., Baccari,C., Chu,A.M., Williamson,M.S. and Brown,J.M. (2003) Use of a genome-wide approach to identify new genes that control resistance of *Saccharomyces cerevisiae* to ionizing radiation. *Radiat. Res.*, **160**, 14–24.
38. Xu,L., Ajimura,M., Padmore,R., Klein,C. and Kleckner,N. (1995) *NDT80*, a meiosis-specific gene required for exit from pachytene in *Saccharomyces cerevisiae*. *Mol. Cell. Biol.*, **15**, 6572–6581.
39. Cao,L., Alani,E. and Kleckner,N. (1990) A pathway for generation and processing of double-strand breaks during meiotic recombination in *S. cerevisiae*. *Cell*, **61**, 1089–1101.
40. Bishop,D.K., Park,D., Xu,L. and Kleckner,N. (1992) *DMC1*: a meiosis-specific yeast homolog of *E. coli recA* required for recombination, synaptonemal complex formation, and cell cycle progression. *Cell*, **69**, 439–456.
41. Shinohara,A., Ogawa,H. and Ogawa,T. (1992) Rad51 protein involved in repair and recombination in S. cerevisiae is a RecA-like protein. *Cell*, **69**, 457–470.
42. Bishop,D.K. (1994) RecA homologs Dmc1 and Rad51 interact to form multiple nuclear complexes prior to meiotic chromosome synapsis. *Cell*, **79**, 1081–1092.
43. Miyazaki,T., Bressan,D.A., Shinohara,M., Haber,J.E. and Shinohara,A. (2004) In vivo assembly and disassembly of Rad51 and Rad52 complexes during double-strand break repair. *EMBO J.*, **23**, 939–949.
44. Tang,S., Wu,M.K., Zhang,R. and Hunter,N. (2015) Pervasive and essential roles of the Top3-Rmi1 decatenase orchestrate recombination and facilitate chromosome segregation in meiosis. *Mol. Cell*, **57**, 607–621.

45. Allers,T. and Lichten,M. (2001) Differential timing and control of noncrossover and crossover recombination during meiosis. *Cell*, **106**, 47–57.
46. Sun,X., Huang,L., Markowitz,T.E., Blitzblau,H.G., Chen,D., Klein,F. and Hochwagen,A. (2015) Transcription dynamically patterns the meiotic chromosome-axis interface. *Elife*, **4**, e07424.
47. Alani,E., Padmore,R. and Kleckner,N. (1990) Analysis of wild-type and rad50 mutants of yeast suggests an intimate relationship between meiotic chromosome synapsis and recombination. *Cell*, **61**, 419–436.
48. Borner,G.V., Kleckner,N. and Hunter,N. (2004) Crossover/noncrossover differentiation, synaptonemal complex formation, and regulatory surveillance at the leptotene/zygotene transition of meiosis. *Cell*, **117**, 29–45.
49. Sym,M., Engebrecht,J.A. and Roeder,G.S. (1993) ZIP1 is a synaptonemal complex protein required for meiotic chromosome synapsis. *Cell*, **72**, 365–378.
50. Smith,A.V. and Roeder,G.S. (1997) The yeast Red1 protein localizes to the cores of meiotic chromosomes. *J. Cell Biol.*, **136**, 957–967.
51. Yu,H.G. and Koshland,D. (2005) Chromosome morphogenesis: condensin-dependent cohesin removal during meiosis. *Cell*, **123**, 397–407.
52. Guacci,V. and Koshland,D. (2012) Cohesin-independent segregation of sister chromatids in budding yeast. *Mol. Biol. Cell*, **23**, 729–739.
53. Lopez-Serra,L., Lengronne,A., Borges,V., Kelly,G. and Uhlmann,F. (2013) Budding yeast Wapl controls sister chromatid cohesion maintenance and chromosome condensation. *Curr. Biol.*, **23**, 64–69.
54. Ding,D.Q., Sakurai,N., Katou,Y., Itoh,T., Shirahige,K., Haraguchi,T. and Hiraoka,Y. (2006) Meiotic cohesins modulate chromosome compaction during meiotic prophase in fission yeast. *J. Cell Biol.*, **174**, 499–508.
55. Conrad,M.N., Lee,C.Y., Wilkerson,J.L. and Dresser,M.E. (2007) MPS3 mediates meiotic bouquet formation in *Saccharomyces cerevisiae*. *Proc. Natl. Acad. Sci. U.S.A.*, **104**, 8863–8868.
56. Trelles-Sticken,E., Adelfalk,C., Loidl,J. and Scherthan,H. (2005) Meiotic telomere clustering requires actin for its formation and cohesin for its resolution. *J. Cell Biol.*, **170**, 213–223.
57. Trelles-Sticken,E., Loidl,J. and Scherthan,H. (1999) Bouquet formation in budding yeast: initiation of recombination is not required for meiotic telomere clustering. *J. Cell. Sci.*, **112**, 651–658.
58. Conrad,M.N., Lee,C.Y., Chao,G., Shinohara,M., Kosaka,H., Shinohara,A., Conchello,J.A. and Dresser,M.E. (2008) Rapid telomere movement in meiotic prophase is promoted by NDJ1, MPS3, and CSM4 and is modulated by recombination. *Cell*, **133**, 1175–1187.
59. Revenkova,E., Eijpe,M., Heyting,C., Hodges,C.A., Hunt,P.A., Liebe,B., Scherthan,H. and Jessberger,R. (2004) Cohesin SMC1 beta is required for meiotic chromosome dynamics, sister chromatid cohesion and DNA recombination. *Nat. Cell Biol.*, **6**, 555–562.
60. Ito,M., Kugou,K., Fawcett,J.A., Mura,S., Ikeda,S., Innan,H. and Ohta,K. (2014) Meiotic recombination cold spots in chromosomal cohesion sites. *Genes Cells*, **19**, 359–373.
61. Heidinger-Pauli,J.M., Unal,E. and Koshland,D. (2009) Distinct targets of the Eco1 acetyltransferase modulate cohesion in S phase and in response to DNA damage. *Mol. Cell*, **34**, 311–321.
62. Lao,J.P., Cloud,V., Huang,C.C., Grubb,J., Thacker,D., Lee,C.Y., Dresser,M.E., Hunter,N. and Bishop,D.K. (2013) Meiotic crossover control by concerted action of Rad51-Dmc1 in homolog template bias and robust homeostatic regulation. *PLoS Genet.*, **9**, e1003978.
63. Thacker,D., Mohibullah,N., Zhu,X. and Keeney,S. (2014) Homologue engagement controls meiotic DNA break number and distribution. *Nature*, **510**, 241–246.
64. Sjogren,C. and Nasmyth,K. (2001) Sister chromatid cohesion is required for postreplicative double-strand break repair in *Saccharomyces cerevisiae*. *Curr. Biol.*, **11**, 991–995.
65. Hiraoka,Y. and Dernburg,A.F. (2009) The SUN rises on meiotic chromosome dynamics. *Dev. Cell*, **17**, 598–605.